

# Structural analysis of star-forming blue early-type galaxies

## Merger-driven star formation in elliptical galaxies

Koshy George

Indian Institute of Astrophysics, 2nd Block, Koramangala, 560034 Bangalore, India  
e-mail: koshy@iiap.res.in

Received 7 September 2016 / Accepted 3 December 2016

### ABSTRACT

**Context.** Star-forming blue early-type galaxies at low redshift can give insight to the stellar mass growth of  $L_*$  elliptical galaxies in the local Universe.

**Aims.** We wish to understand the reason for star formation in these otherwise passively evolving red and dead stellar systems. The fuel for star formation can be acquired through recent accretion events such as mergers or flyby. The signatures of such events should be evident from a structural analysis of the galaxy image.

**Methods.** We carried out structural analysis on SDSS  $r$ -band imaging data of 55 star-forming blue elliptical galaxies, derived the structural parameters, analysed the residuals from best-fit to surface brightness distribution, and constructed the galaxy scaling relations.

**Results.** We found that star-forming blue early-type galaxies are bulge-dominated systems with axial ratio  $>0.5$  and surface brightness profiles fitted by Sérsic profiles with index ( $n$ ) mostly  $>2$ . Twenty-three galaxies are found to have  $n < 2$ ; these could be hosting a disc component. The residual images of the 32 galaxy surface brightness profile fits show structural features indicative of recent interactions. The star-forming blue elliptical galaxies follow the Kormendy relation and show the characteristics of normal elliptical galaxies as far as structural analysis is concerned. There is a general trend for high-luminosity galaxies to display interaction signatures and high star formation rates.

**Conclusions.** The star-forming population of blue early-type galaxies at low redshifts could be normal ellipticals that might have undergone a recent gas-rich minor merger event. The star formation in these galaxies will shut down once the recently acquired fuel is consumed, following which the galaxy will evolve to a normal early-type galaxy.

**Key words.** galaxies: elliptical and lenticular, cD – galaxies: evolution – galaxies: star formation – galaxies: structure

## 1. Introduction

Early-type galaxies (ETGs) in the local Universe are morphologically ellipticals or lenticulars with little or no ongoing star formation, host evolved stellar population, and populate the red sequence on the galaxy colour–magnitude diagram (Faber 1973; Visvanathan & Sandage 1977; Baldry et al. 2004). Early-type galaxies populate the massive end of the galaxy stellar mass function at least from redshift ( $z$ )  $\sim 1$  and constitute a significant fraction of the stellar mass in the local Universe. Recent observations suggest that the stellar mass of field  $L_*$  ETGs almost doubled from  $z \sim 1$  to 0 (Bell et al. 2004; Faber et al. 2007; Brown et al. 2007). The observed increase of stellar mass in  $L^*$  ETGs between  $z \sim 1$  to 0 is in accordance with the current paradigm of  $\Lambda$ CDM cosmology, which predicts hierarchical formation and evolution for galaxies (De Lucia et al. 2006).

Galaxies follow different evolutionary paths over the last 8 billion years to account for the observed growth in stellar mass. The galaxies can be at different stages of the evolutionary path, which at different redshifts and varying environments can be used to test our current understanding of galaxy formation and evolution (Faber et al. 2007, for a detailed description of the various galaxy evolutionary paths). Star-forming blue spiral galaxies in the absence of continuous supply of molecular gas can quench star formation and migrate from the star-forming blue cloud to the passively evolving red sequence on the galaxy colour–magnitude diagram. Major mergers between two star-forming spiral galaxies go through a morphological destructive phase

with intense star formation that depletes the gas reservoir and makes the merger remnant an ETG on the red sequence (Toomre 1977). Major mergers are more common at high redshift when the Universe was less than half of the current age (Conselice et al. 2003). Minor mergers, on the other hand, are more frequent and can contribute to the continuous build-up of galaxies in the local Universe (Kaviraj et al. 2009; Kaviraj 2014). The slow build-up of the outer galaxy until the present epoch, as observed in the size evolution of elliptical galaxies, is now believed to be due to minor mergers (Trujillo et al. 2011). Minor mergers can also bring gas and induce star formation in an otherwise gas-poor elliptical galaxy. HI surveys of relaxed nearby elliptical galaxies demonstrate the presence of significant amounts of neutral hydrogen, the origin of which is attributed to external sources like minor mergers (Morganti et al. 2006; Oosterloo et al. 2010; Serra et al. 2014). The processes responsible for bringing gas to elliptical galaxies can be mergers or gas accretion from the intergalactic medium. Star formation can occur from this gas and can account for some of the stellar mass build-up in ETGs. Galaxies can then move from the red sequence to the blue cloud on the galaxy colour–magnitude diagram.

The report of a sample of blue star-forming ETGs is interesting in this context (Schawinski et al. 2009, hereafter S09). The elliptical morphology of these  $L_*$  galaxies is based on visual classifications from the Galaxy Zoo (GZ). They are found in low-density environments and also make up  $5.7 \pm 0.4\%$  of the low-redshift ETG population.

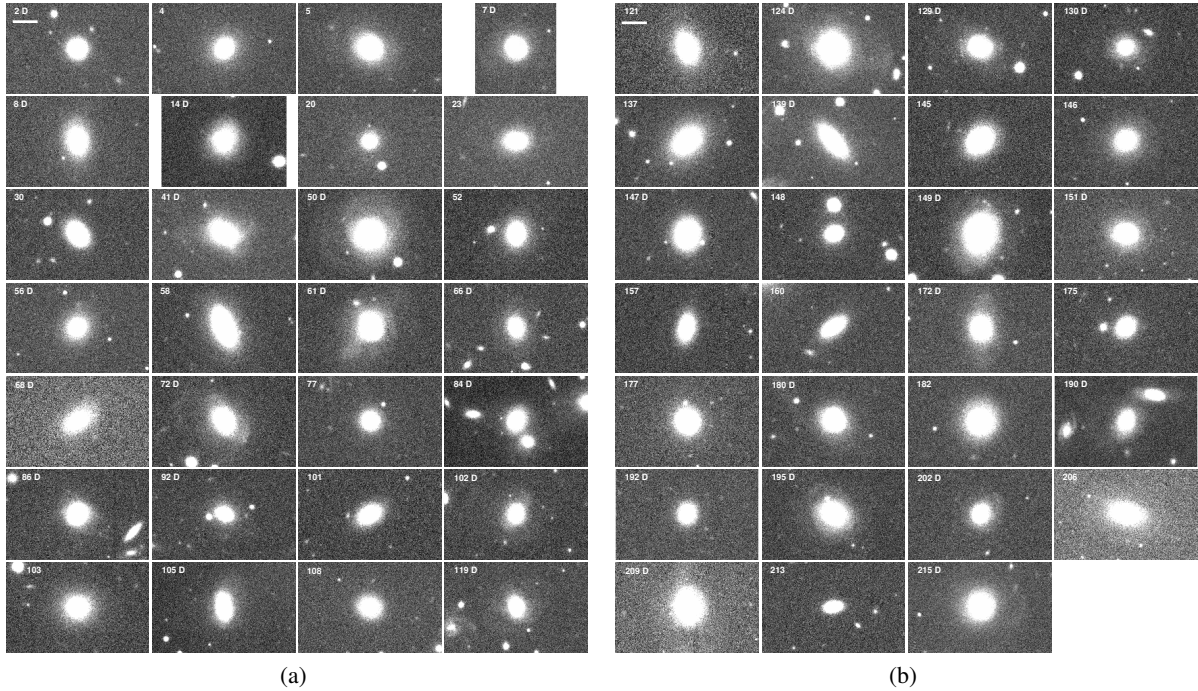


**Fig. 1.** SDSS  $r$ -band images of 55 star-forming blue ETGs taken with 54s integration time. Note the faint features at the galaxy outskirts with shallow SDSS imaging. The S09 object identification number is given at the top of each image. The images showing the presence of recent interaction features in residual analysis are marked with D. All images are of the same dimension, and a line of length  $15''$  is shown in the first image; this corresponds to the typical size of the galaxy.

Blue ellipticals have an  $r$ -band absolute magnitude ( $M_r$ )  $< -20.5$  and  $-r$  colour  $< 2.5$  mag. Based on the positions on the line diagnostic diagram (Baldwin et al. 1981), S09 have classified 25% as only star-forming, 25% as both star-forming and active galactic nucleus (AGN), 12% as AGN and 38% as having no strong emission lines to classify. The star formation rates (SFR) of galaxies are estimated from the  $H\alpha$  line luminosity using the calibration of (Kennicutt 1998, see S09 for a comparison of SFR estimated with other proxies). The 55 purely star-forming blue ETGs (out of a total of 204 blue ETGs) have high SFR (0.45 to  $21 M_{\odot}/\text{yr}$ ) and very blue colours for any such systems found in the local Universe. Few of these systems are reported as ongoing or recently interacting galaxies (George & Zingade 2015). The 55 star-forming blue ETGs are used in this study to understand the existence of such systems in the current paradigm of galaxy formation and evolution. We address the following points: we confirm the elliptical nature, the triggering mechanism of star formation in an otherwise red and dead elliptical galaxy, the availability of fuel for star formation, and the fate of blue ETGs. Structural analysis can give insights into the underlying morphology of these objects, and the estimation of structural parameters allows us to make galaxy scaling relations. We first establish the elliptical nature of blue ETGs by a detailed structural analysis and place these systems in the context of galaxy scaling relations. We adopt a flat Universe cosmology with  $H_0 = 71 \text{ km s}^{-1} \text{ Mpc}^{-1}$ ,  $\Omega_M = 0.27$ ,  $\Omega_{\Lambda} = 0.73$  (Komatsu et al. 2011).

## 2. Data

The SDSS DR7 Abazajian et al. (2009)  $r$ -band images of 55 star-forming blue ETGs from S09 were used for the structural analysis. We used the structural parameters data from the catalogue of Meert et al. (2015), which is constructed by applying

two-dimensional point-spread function (PSF) corrected surface brightness profile fits of  $7 \times 10^5$  spectroscopically selected galaxies from SDSS DR7. The fitting routine GALFIT (Peng et al. 2002) and analysis pipeline PyMorph (Vikram et al. 2010) were used to estimate the structural parameters. The choice of fitting the model (single or double) components to the galaxies to measure the total magnitude and half-light radius was extensively tested based on simulations of mock galaxies by Meert et al. (2013). The authors concluded that a Sérsic + exponential component can optimally measure the galaxy global parameters across many galaxy types. Hence we used the structural parameters estimated with surface brightness profile fitting with a double component, Sérsic (Sérsic 1968), and an exponential profile to perform a best fit on the galaxy surface brightness distribution. The measured total magnitude, effective radius, Sérsic index, and the ratio between the major and the minor axis (axial ratio  $b/a$ ) of the galaxy brightness distribution were used. We further analysed the residual data from the profile fitting results for a detailed structural study (residual images from a priv. comm. with Alan Meert). We also used the structural parameters estimated with a surface brightness profile fitting using a single Sérsic profile to derive the galaxy global parameters and check the dependence of the choice on the number of components that affect our residual analysis.

## 3. Structural analysis

### 3.1. Star-forming blue early-type galaxies

The SDSS  $r$ -band imaging data of 55 star-forming blue ETGs in the blue cloud were visually inspected for any signs of recent interaction. We found that many galaxies show features at high galactic radii that are indicative of recent interactions. Figure 1 shows the  $r$ -band images of 55 blue ETGs. The galaxies with ObjID 41, 50, 56, 61, 72, 124, 129, 149, 172, 195, and

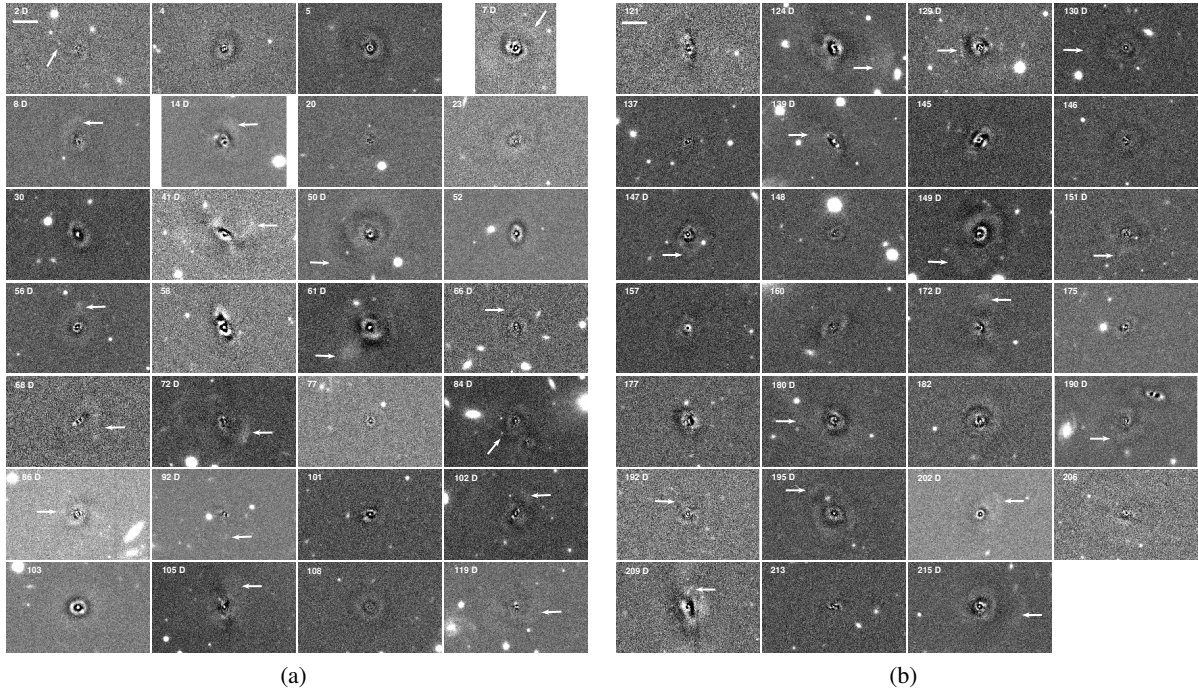


**Fig. 2.** Residuals of Sérsic + exponential fit to SDSS  $r$ -band images of 55 star-forming blue ETGs from Meert et al. (2015). The S09 object identification number is given at the top of each image. The galaxy residual images showing the presence of recent interaction features are marked with D, indicating the presence of stellar debris. All images are of the same dimension, and a line of length  $15''$  is shown in the first image; this corresponds to the typical size of the galaxy. The location of the stellar debris feature is indicated with an arrow.

215 show features at the galaxy outskirts in  $r$ -band images taken with 54s integration time. It is our interest to understand the origin of these features, which can shed light on the formation of the blue ETGs. The visual analysis of  $r$ -band images was further corroborated with the residuals of surface brightness profile fits on the galaxy images. We analysed the difference image obtained from the best-fit model and the galaxy image, which is the residuals to the profile fits. The visual analysis of the residual images of 55 star-forming galaxies clearly shows the deviation from a smooth featureless galaxy surface brightness profile typical of elliptical galaxies. Figure 2 shows the residuals from a Sérsic + exponential profile fit to the SDSS  $r$ -band images as explained in Meert et al. (2015). Analysing the residual image, we found that in addition to signatures of recent interactions, there are indications of deviations from a smooth featureless early-type morphology with galaxies hosting tidal tails, shells, asymmetric excess light far of and near to the galactic centre, which we collectively call stellar debris. We note that the residual images show a point source at the central region of the galaxy along with a ring structure, which demonstrates the failure of a simple two-component model to fit the underlying nature of the surface brightness profiles of blue ETGs. The normal ETGs from the catalogue of Meert et al. (2015) do not show such features in the residual images, as demonstrated in Fig. 2 of Meert et al. (2013). Blue ETGs appear to have more structural inhomogeneities than normal ETGs. We also checked the residual images from a single Sérsic component fit to the galaxy surface brightness distribution, and the interaction features remains, regardless of the number of components used to model the galaxy surface brightness profile. We found that out of 55 blue ETGs, 32 galaxies show features that are indicative of recent merger events in the residual images, which we interpret as stellar debris. Table A.1 provides the details of the structural

analysis based on visual inspection of the residual images along with details of the galaxy  $u - r$  colours and star formation rates. We note that deep imaging of these galaxies is expected to reveal low surface brightness features that are otherwise not recorded in shallow SDSS images taken with 54s integration time.

Nair & Abraham (2010) presented a detailed study of the morphology and the presence of fine structures (including interaction signatures such as tails, shells, and collisional rings) based on visual classifications for 14 034 galaxies in the Sloan Digital Sky Survey (SDSS) data release 4 (DR4) for the redshift range,  $0.01 < z < 0.1$  and  $g$ -band magnitude  $< 16$  mag. We note that 25 galaxies (brighter than  $g \sim 16$  mag) in our sample of 55 blue ETGs are reported in their catalogue with galaxy details. Four galaxies are classified as with S0 and 21 with E morphology. The galaxy with ObjID 58 is classified with an Sa morphology. The number of galaxies listed with interaction features in their study are different (10) from our residual analysis (21), which is based on image decomposition. We note here in particular the galaxies with objIds 50 and 215, which show signs of interaction in our residual analysis (Fig. 2), but are not reported in the analysis of Nair & Abraham (2010).

Galaxy Zoo classifications of blue ETGs are done purely based on visual morphology, and only those galaxies that secure  $> 80\%$  votes are selected for the clean sample, as described in S09. This does not exclude S0 galaxies from our sample of 55 star-forming blue ETGs, and as described in S09, a few of our galaxies can have an S0 morphology. We call our sample ETGs, which includes both ellipticals and S0s. The bias in the GZ classification process had been statistically studied by Bamford et al. (2009), who showed that contamination from other morphological types (particularly spirals) is 4%, and for our star-forming blue ETGs, this translates into 2 galaxies. It therefore follows

that one of our galaxies is classified with an Sa morphology in the list of 25 blue ETGs from [Nair & Abraham \(2010\)](#).

The very recent galaxy morphology classification from Galaxy Zoo 2 supercedes the original GZ and compiles the morphologies for galaxies in the SDSS DR7 along with deeper images from Stripe 82 ([Willett et al. 2013](#)). Fifty-two galaxies (from our sample of 55 star-forming blue ETGs) in the GZ2 catalogue have a smooth morphology, which confirms the original GZ classification.

### 3.2. Normal early-type galaxies

The structural analysis of blue ETGs shows features that are indicative of recent interactions. The interesting question is how common these features are for normal ETGs on the red sequence of the galaxy colour–magnitude diagram. Tidal features are reported for ETGs on the red sequence for galaxies with an  $r$ -band absolute magnitude  $M_r < -20.5$  in the redshift range  $z < 0.05$  by visual inspection of the SDSS Stripe82 imaging data by [Kaviraj \(2010\)](#). The SDSS Stripe 82 imaging is  $\sim 2$  mag deeper than the normal SDSS  $r$ -band imaging and hence is an ideal data set in which to search for faint features that are indicative of recent interactions around ETGs that are otherwise not seen in the shallow SDSS imaging (and which can be revealed without an image decomposition technique). The galaxies reported by [Kaviraj \(2010\)](#) consist of 238 relaxed ETGs without any morphological disturbances and 67 ETGs with tidal features exhibiting shells, fans, tidal tails, and dust lanes at the depth of the Stripe82 images. The analysis based on the position of galaxies on the BPT diagram ([Baldwin et al. 1981](#)) shows that 1.3% of the relaxed ETGs and 4.5% of the ETGs with tidal features and dust lanes host ongoing star formation. However, the ETG populations with relaxed and the tidal features have a similar distributions in  $(u-r)$  colour (median  $\sim 2.5$  mag), indicating that any triggered star formation that is due to the interaction is weak and did not change the optical colours. The recent interaction may not have brought an amount of gas sufficient for star formation to change the colours of these galaxies, as in the case of star-forming blue ETGs. It is worth noting that only  $28 \pm 3\%$  of the galaxies from the deeper Stripe 82 imaging data of [Kaviraj \(2010\)](#) show features that are indicative of recent interaction, whereas  $58 \pm 7\%$  of blue ETGs (with normal SDSS imaging) have interaction features in residual analysis. The uncertainties are calculated from considering the galaxy sample following a binomial probability distribution.

The tidal features are more common around massive galaxies (stellar mass  $> 10^{10.5} M_\odot$ ), and galaxies on the red sequence are twice as likely to show tidal features than galaxies in the blue cloud ([Atkinson et al. 2013](#)). The presence of tidal features around galaxy images depends on the depth of the data, and as summarised in Table 3 of [Kim et al. \(2012\)](#), deeper imaging data retrieve more tidal features around ETGs. We expect a similar trend for blue ETGs in data from deep imaging ( $\sim 2$  mag lower than SDSS) surveys like the DECam Legacy Survey of the SDSS Equatorial Sky (DECaLS). It has been demonstrated that the probability of finding features around blue ETGs is in general higher than for normal ETGs with deeper imaging data.

### 3.3. Enhanced star formation rate and presence of tidal debris

The presence of stellar debris in the residual images of galaxies can be interpreted as an indication of recent galaxy-scale

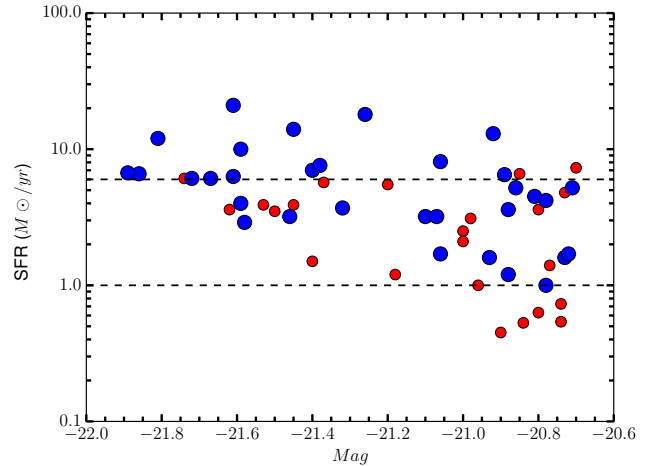


**Fig. 3.** SFR of 55 star-forming blue ETGs plotted against the galaxy  $r$ -band absolute magnitude. Galaxy with interaction features are shown in blue and those without detected features in red. Galaxies are separated into three SFR bins using the dotted lines at 1 and  $6 M_\odot/\text{yr}$ .

interactions. The detailed knowledge of the mass ratios, stellar population content, and the gas exchanged during these galaxy-scale interaction is crucial for our understanding of the formation and evolution of blue ETGs. We are interested in knowing the influence of recent interaction on the ongoing star formation in blue ETGs. We therefore investigated the SFR of the blue ETGs with and without stellar debris in the residual images. We performed a Kolmogorov-Smirnov (KS) test on the SFR of galaxies with and without stellar debris in residual images and found that with a 95.73% probability, they are drawn from two different galaxy distributions. This clearly indicates that galaxies with stellar debris show a different trend in star formation rate from galaxies without detected features. The  $r$ -band absolute magnitude (based on SDSS petromag, which measures the total light of the galaxy) of blue ETGs is plotted against the SFR in Fig. 3. Blue ETGs with stellar debris identified in the residual analysis are shown in blue and those without detected features in red. We divided the galaxies into three bins of SFR:  $SFR < 1$ , 1 to 6, and  $> 6 M_\odot/\text{yr}$ . Blue ETGs with  $SFR < 1 M_\odot/\text{yr}$  show no features that would be indicative of recent interaction (5 galaxies), whereas galaxies of SFR 1 to  $6 M_\odot/\text{yr}$  are a mix of galaxies with (17 galaxies) and without (15 galaxies) tidal features. Finally, the  $> 6 M_\odot/\text{yr}$  region is dominated (15/18) by galaxies with tidal interaction features. We note that there is a general trend for galaxies with higher luminosity to display interaction signatures and high SFR, as confirmed with a KS test. The high SFR are responsible for the higher luminosity of these galaxies, and based on the position of galaxies in the SFR plot, we argue that the recent interaction might have brought in the sufficient fuel (cold molecular hydrogen gas or molecular gas) for the observed intense SFR in an otherwise normal elliptical galaxy. The galaxies with high SFR might have acquired the gas very recently, where the intense ongoing star formation makes the galaxies both bluer and brighter. The SFR and the absolute magnitude will decrease and the colour will increase depending on the depletion of molecular gas (once acquired from interaction) and will decide the fate of the blue ETG.

## 4. Scaling relations of blue early-type galaxies

The Kormendy relation is a scaling relation observed between the effective radii  $R_e$  (kpc) and the mean surface brightness at the

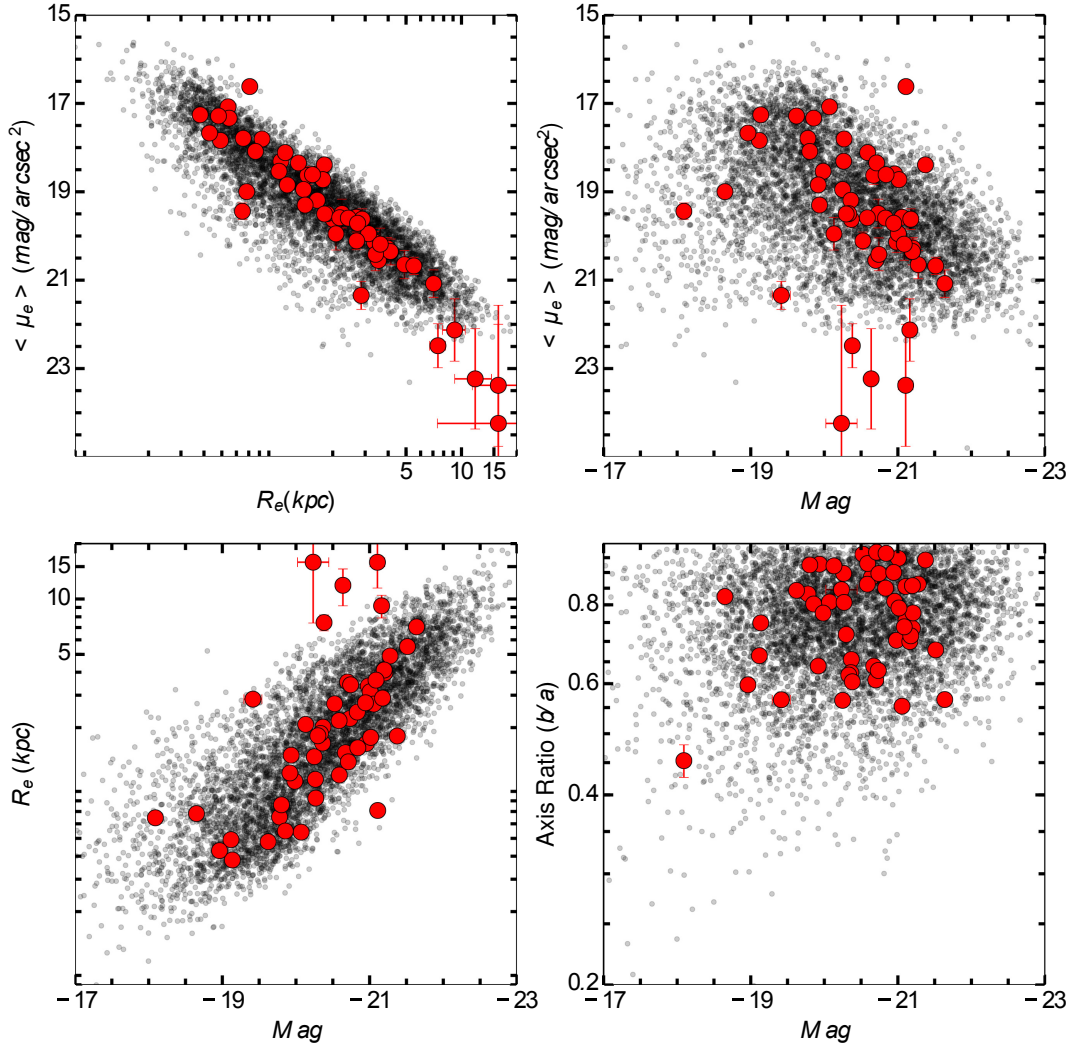


**Fig. 4.** 55 star-forming blue ETGs on the galaxy scaling relations. The parameters used in the diagram are derived from the  $r$ -band SDSS imaging data. Grey points are normal elliptical galaxies in the redshift range  $0.02 > z > 0.05$ .

effective radius  $\langle \mu_e \rangle$  ( $\text{mag}/\text{arcsec}^2$ ) of ETGs (Kormendy 1977). The ETGs in all environments are found to follow this tight relation up to redshift  $\sim 1$  (La Barbera et al. 2003; Reda et al. 2004; di Serego Alighieri et al. 2005). The circularised effective radius is first computed from the measured effective radius ( $a_e$ ) and axial ratio ( $b/a$ ) using the equation  $R_e = a_e \sqrt{b/a}$ . The mean surface brightness is calculated from the circularised effective radius (arcsec), total magnitude (mag), and redshift ( $z$ ) using the following equation:

$$\langle \mu_e \rangle = \text{mag} + 2.5 \log(2\pi R_e^2) - 10 \log(1+z).$$

The mean surface brightness  $\langle \mu_e \rangle$ , effective radii  $R_e$  (kpc), axial ratio  $b/a$ , and total magnitude (mag) is used to construct the scaling relations of blue ETGs.

#### 4.1. Double-component case: Sérsic + exponential profile

We constructed the Kormendy relation of star-forming blue ETGs using the measured structural parameters from a double-component model fit to the galaxy surface brightness distribution. Figure 4 shows the  $r$ -band structural parameters of 55 blue ETGs on the scaling relations. We also plot the scaling relation of normal elliptical galaxies in the redshift range  $0.02 > z > 0.05$  from the Meert catalogue (in grey) along

with the 55 star-forming blue ETGs (red). We selected only those galaxies that are morphologically ellipticals confirmed from GalaxyZoo (Lintott et al. 2008) to assemble the normal elliptical galaxy list. It is clear from figure that blue ETGs and normal elliptical galaxies share similar structural properties. The Sérsic index of the 55 blue ETGs is shown in Fig. 5.

Two galaxies (ObjID 30 157) are having unrealistic errors in the measured structural parameters and hence we did not use them when we constructed the scaling relation. We note that 5 galaxies (ObjId 52, 103, 105, 139, 148) have low surface brightness and high effective surface brightness for their measured absolute magnitude. These 5 galaxies have high Sérsic index values (saturating at  $n \sim 8$ ). There are 23 galaxies with Sérsic index values  $< 2$ , which implies that they are disc systems. The size-magnitude relation of normal ellipticals and blue ellipticals shows the similar trend. Blue ETGs are bulge-dominated systems with  $b/a$  values greater than 0.5, which further confirms the morphological classification.

#### 4.2. Single-component case: Sérsic profile

We also constructed the scaling relation using the galaxy structural parameters estimated with the single Sérsic model fit to the surface brightness distribution. The 55 blue ETGs fall on

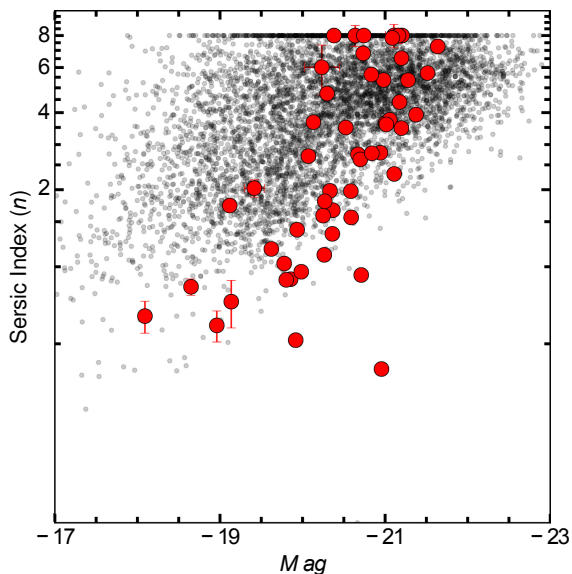


**Fig. 5.** Sérsic index ( $n$ ) of 55 star-forming blue ETGs plotted against the  $r$ -band absolute magnitude. The parameters used in the diagram are derived from the  $r$ -band SDSS imaging data. Grey points are normal elliptical galaxies in the redshift range  $0.02 > z > 0.05$ .

the scaling relation along with normal elliptical galaxies. We note that for the single Sérsic component case, 9 galaxies have a Sérsic index value  $< 2$  and 3 have a Sérsic index saturating at index value 8. We checked the  $r$ -band images and the residual images of the low Sérsic index galaxies and conclude with the following inferences. For the galaxies with ObjID 7 and 58, the galaxy image is in the corner of the fitting box region and the fitting process may be affected by this artefact. The galaxies with ObjID 30, 52, 157, 180, and 213 show features in the residual images that are indicative of an intrinsic disc nature of the galaxy. The galaxy with ObjID 148 has a bright object nearby that might affect the fitting process. The galaxy with ObjID 101 shows a patch in the residual images that might be due to the presence of dust lanes. The galaxies with a Sérsic index value 8, with objId 14 and 146, have a point source in the centre region of the residual images that is suggestive of a steep core, and the galaxy with ObjID 84 has bright objects nearby that affect the fitting process.

The main inferences from the scaling relation of star-forming blue ETGs are the following: blue ETGs obey the Kormendy relation and the size-magnitude relation of normal (red and dead) elliptical galaxies. The stellar population content may be different (with blue colours and ongoing star formation), but the structure and the dynamical state of blue ETGs are comparable to normal elliptical galaxies in the local Universe. The double-component fits (Sérsic + exponential) shows galaxies with low Sérsic index values following a shallow declining light distribution in contrast to the steep distribution of the single-component case (see Table A.1). We infer that this is due to the presence of a disc component in a good fraction (23/55) of blue ETGs where star formation might be occurring. The star formation in blue ETGs is expected to be due to recent events that occurred in a normal elliptical galaxy that did not alter the overall morphological structure of the galaxy. It is therefore worth investigating events in the local Universe that can cause star formation without disturbing the structure of a normal elliptical galaxy.

## 5. Discussion

The position of star-forming blue ETGs on the colour–magnitude/colour–stellar mass diagrams has been interpreted as possible migration from the red sequence to the blue cloud after acquiring sufficient fuel for star formation or fading post-starburst galaxies (Kannappan et al. 2009; Huertas-Company et al. 2010; Thilker et al. 2010; Marino et al. 2011; Moffett et al. 2012, 2015; McIntosh et al. 2014; Rutkowski et al. 2014; Wong et al. 2015). The sample of a few blue ETGs from other studies was found to host a significant amount of molecular gas ( $\sim 10^{7-9} M_{\odot}$ ) with a linear dependence on star formation surface density within the galaxy and a higher molecular gas star formation efficiency than in normal star-forming late-type galaxies (Wei et al. 2010; Stark et al. 2013). The higher efficiency in converting the molecular gas to stars is expected to rapidly deplete the fuel for star formation, and in the absence of an external supply of fresh gas, the galaxy can rapidly change to a normal red and dead ETG. Stark et al. (2013) analysed the relationship between mass-corrected blue centredness (tracing recent enhancements of central star formation) and total molecular-to-atomic ( $H_2/HI$ ) gas ratios for early- to late-type field galaxies with stellar masses of  $\sim 10^{7.2-11.2} M_{\odot}$ . Blue ETGs are found to follow a different relation (compared to spiral galaxies, for which a positive correlation exists, which is interpreted as a result of local galaxy interactions and molecular gas supply) and are found to be late or starburst merger remnants with the starburst (keeping the centre blue) rapidly depleting the molecular gas. We consider the extreme case of our sample with star formation rate of  $21 M_{\odot}/\text{yr}$  holding molecular gas content of  $\sim 10^9 M_{\odot}$  as seen in other studies of blue ETGs (Wei et al. 2010; Stark et al. 2013). If we consider a 50% molecular gas star formation efficiency, then half of the molecular gas content will be converted into stars in  $10^8$  yr. The gas content will be completely exhausted in  $2 \times 10^8$  yr and will change the blue ETG back to a normal galaxy on the red sequence (in  $< 1$  Gyr timescale). Blue ETGs would then be a transient phase in the evolution of a normal ETG and explain why they contribute only a low fraction ( $5.7 \pm 0.4\%$ ) to the low-redshift ETG population.

We found that 58% of the star-forming blue ETGs host signatures of recent interactions and fall, along with normal ellipticals, on the galaxy scaling relations. This demonstrated that the sample of 55 galaxies has characteristics of normal elliptical galaxies except for the high SFR and blue colours. We suggest that the star formation seen in these otherwise passively evolving red and dead stellar systems is related to the recent interactions. The intense star formation found in these galaxies needs a huge reservoir of molecular gas (particularly for those galaxies with high SFR that reach as high as  $21 M_{\odot}/\text{yr}$ ), which is generally not available in intrinsically gas-poor elliptical galaxies (Young et al. 2011, 2014). We invoke the scenario of a recent interaction with a gas-rich galaxy that could provide the fuel for intense star formation along with the imprint of interaction in the form of tidal tails and stellar debris. The nature of the interaction could be a major merger (1/1 in mass ratio), minor merger ( $< 1/3$  in mass ratio), or a fly-by, depending on the strength of the tidal features and the dynamical state of the galaxy.

The ETGs in the local Universe are known to host a low level of recent star formation (Trager et al. 2000; Yi et al. 2005), and there is accumulating evidence that indicates that minor mergers are responsible for this low-level star formation (Kaviraj et al. 2009, 2011; Kaviraj 2014). The majority of ETGs in the local Universe are found to have signatures of recent interaction and a low level of recent star formation (Kaviraj 2010). The

recent interaction may have provided the fuel for the observed low level of star formation. The reported ETGs in low-density environment with reservoirs of neutral hydrogen in regular rotating discs and extended morphologies further support this argument (Serra & Oosterloo 2010). Numerical simulations have also demonstrated the occurrence of gas rings and the accretion of fresh gas in ETGs from minor mergers (Mapelli et al. 2015; Kaviraj et al. 2009; Peirani et al. 2010).

The formation of shells and tidal tails has been reproduced in  $N$ -body simulations of galaxy minor mergers (Quinn 1984; Feldmann et al. 2008). Feldmann et al. (2008) were able to reproduce the types of tidal features we observed here with mass ratios of 1:10 between the accreting elliptical and the accreted disc galaxy. The authors argued that mergers between a disc galaxy and an elliptical galaxy can form tidal features that last for  $\sim 2$  Gyr in comparison to mergers between equal-mass galaxies, which lasts for a few million years.

The connection between the star-forming blue ETG and polar-ring galaxies in the local Universe is worth investigating. A polar-ring galaxy system consists of a gas-poor S0 galaxy with a gas-rich star-forming polar ring held perpendicular to the semi-major axis of host galaxy (Whitmore et al. 1990). The favoured scenario of the polar-ring formation is the accretion of a gas-rich dwarf galaxy by an ETG (Bournaud & Combes 2003). The polar ring of the galaxy is found to be stable, young, and gas rich (molecular gas mass of the range  $\sim 10^{10} M_{\odot}$ ) compared to the old, gas-poor host galaxy (Galletta et al. 1997; van Driel et al. 2000, 2002; Iodice et al. 2002a,b,c; Combes et al. 2013). We consider the case where the central host galaxy is replaced by a normal gas poor elliptical galaxy, which is then allowed to interact with a gas-rich dwarf galaxy. The system may not be stable like in the case of a polar-ring galaxy, but instead results in the formation of a gas-rich elliptical galaxy with intense star formation from the freshly acquired gas, showing signs of recent interaction in the form of tidal tails and shells. The end product of this scenario is a blue ETG with the characteristics of the galaxies we studied here.

We have considered possible triggers of star formation in an otherwise red and dead elliptical galaxy. While we cannot point to one compelling source, we showed signatures of recent interaction in images of galaxies with high SFR, and we suggest that the interaction with a gas-rich companion could have triggered the star formation in elliptical galaxies. (We note that the interaction features have been detected around images of blue ETGs with low SFR and also around normal galaxies.) The interaction with the gas-rich companion may have provided the fuel for star formation. Star formation occurs in discs where gas settles and stabilises. We showed signatures of disc component in 23 blue ETGs from the structural analysis. The star-forming phase might be transient ( $< 1$  Gyr), which is supported by the low fraction of such galaxies in the local Universe. The intense star formation rate, in the absence of a continuous supply of molecular gas, will rapidly deplete the fuel for further star formation. Blue ETGs will then move from the blue cloud to the red sequence on the galaxy colour–magnitude diagram. The transient path in the evolution of a normal elliptical galaxy will then contribute to the build-up of the stellar mass of ETGs in the local Universe.

## 6. Summary

We presented a structural analysis of the SDSS  $r$ -band imaging data of 55 star-forming blue ETGs. We found that the residuals of the 32 galaxy surface brightness profile fits show structural features that are indicative of recent interactions. Galaxies

with higher luminosity display interaction signatures and high SFR. The star-forming blue ETGs follow the Kormendy relation and show characteristics of normal elliptical galaxies on the galaxy scaling relations. The star-forming population of blue ETGs at low redshifts could be normal ellipticals that may have undergone a recent minor-merger event. The star formation in these galaxies will shut down once the recently acquired fuel is consumed, and the galaxies will evolve into normal ETGs. Blue ETGs are probably transient systems that are depleted of the fuel for star formation and become a normal ETG there by increasing the stellar mass on the red sequence in the local Universe.

*Acknowledgements.* We are grateful to the referee for critical comments that improved the quality of the paper. We thank Alan Meert for the blue early-type galaxy residual images and Sugata Kaviraj for the catalogue on peculiar early-type galaxies in the Sloan Digital Sky Survey Stripe82. Funding for the SDSS and SDSS-II has been provided by the Alfred P. Sloan Foundation, the Participating Institutions, the National Science Foundation, the U.S. Department of Energy, the National Aeronautics and Space Administration, the Japanese Monbukagakusho, the Max Planck Society, and the Higher Education Funding Council for England. The SDSS Web Site is <http://www.sdss.org/>. The SDSS is managed by the Astrophysical Research Consortium for the Participating Institutions. The Participating Institutions are the American Museum of Natural History, Astrophysical Institute Potsdam, University of Basel, University of Cambridge, Case Western Reserve University, University of Chicago, Drexel University, Fermilab, the Institute for Advanced Study, the Japan Participation Group, Johns Hopkins University, the Joint Institute for Nuclear Astrophysics, the Kavli Institute for Particle Astrophysics and Cosmology, the Korean Scientist Group, the Chinese Academy of Sciences (LAMOST), Los Alamos National Laboratory, the Max-Planck-Institute for Astronomy (MPIA), the Max-Planck-Institute for Astrophysics (MPA), New Mexico State University, Ohio State University, University of Pittsburgh, University of Portsmouth, Princeton University, the United States Naval Observatory, and the University of Washington.

## References

- Abazajian, K. N., Adelman-McCarthy, J. K., Agüeros, M. A., et al. 2009, *ApJS*, **182**, 543
- Atkinson, A. M., Abraham, R. G., & Ferguson, A. M. N. 2013, *ApJ*, **765**, 28
- Baldry, I. K., Glazebrook, K., Brinkmann, J., et al. 2004, *ApJ*, **600**, 681
- Baldwin, J. A., Phillips, M. M., & Terlevich, R. 1981, *PASP*, **93**, 5
- Bamford, S. P., Nichol, R. C., Baldry, I. K., et al. 2009, *MNRAS*, **393**, 1324
- Bell, E. F., Wolf, C., Meisenheimer, K., et al., 2004, *ApJ*, **608**, 752
- Bournaud, F., & Combes, F. 2003, *A&A*, **401**, 817
- Brown, M. J. I., Dey, A., Jannuzi, B. T., et al. 2007, *ApJ*, **654**, 858
- Combes, F., Moiseev, A., & Reshetnikov, V. 2013, *A&A*, **554**, A11
- Conselice, C. J., Bershad, M. A., Dickinson, M., & Papovich, C. 2003, *AJ*, **126**, 1183
- De Lucia, G., Springel, V., White, S. D. M., Croton, D., & Kauffmann, G. 2006, *MNRAS*, **366**, 499
- di Serego Alighieri, S., Vernet, J., Cimatti, A., et al. 2005, *A&A*, **442**, 125
- Faber, S. M. 1973, *ApJ*, **179**, 731
- Faber, S. M., Willmer, C. N. A., Wolf, C., et al. 2007, *ApJ*, **665**, 265
- Feldmann, R., Mayer, L., & Carollo, C. M. 2008, *ApJ*, **684**, 1062
- Galletta, G., Sage, L. J., & Sparke, L. S. 1997, *MNRAS*, **284**, 773
- George, K., & Zingade, K. 2015, *A&A*, **583**, A103
- Huertas-Company, M., Aguerrí, J. A. L., Tresse, L., et al. 2010, *A&A*, **515**, A3
- Iodice, E., Arnaboldi, M., De Lucia, G., et al. 2002a, *AJ*, **123**, 195
- Iodice, E., Arnaboldi, M., Sparke, L. S., Gallagher, J. S., & Freeman, K. C. 2002b, *A&A*, **391**, 103
- Iodice, E., Arnaboldi, M., Sparke, L. S., & Freeman, K. C. 2002c, *A&A*, **391**, 117
- Kannappan, S. J., Guie, J. M., & Baker, A. J. 2009, *AJ*, **138**, 579
- Kaviraj, S. 2010, *MNRAS*, **408**, 170
- Kaviraj, S. 2014, *MNRAS*, **437**, L41
- Kaviraj, S., Peirani, S., Khochfar, S., Silk, J., & Kay, S. 2009, *MNRAS*, **394**, 1713
- Kaviraj, S., Tan, K.-M., Ellis, R. S., & Silk, J. 2011, *MNRAS*, **411**, 2148
- Kennicutt, R. C., Jr. 1998, *ApJ*, **498**, 541
- Kim, T., Sheth, K., Hinz, J. L., et al. 2012, *ApJ*, **753**, 43
- Komatsu, E., Smith, K. M., Dunkley, J., et al., 2011, *ApJS*, **192**, 18
- Kormendy, J. 1977, *ApJ*, **218**, 333

- La Barbera, F., Busarello, G., Merluzzi, P., Massarotti, M., & Capaccioli, M. 2003, *ApJ*, **595**, 127
- Lintott, C. J., Schawinski, K., Slosar, A., et al. 2008, *MNRAS*, **389**, 1179
- Mapelli, M., Rampazzo, R., & Marino, A. 2015, *A&A*, **575**, A16
- Marino, A., Bianchi, L., Rampazzo, R., et al. 2011, *ApJ*, **736**, 154
- McIntosh, D. H., Wagner, C., Cooper, A., et al. 2014, *MNRAS*, **442**, 533
- Meert, A., Vikram, V., & Bernardi, M. 2013, *MNRAS*, **433**, 1344
- Meert, A., Vikram, V., & Bernardi, M. 2015, *MNRAS*, **446**, 3943
- Morganti, R., de Zeeuw, P. T., Oosterloo, T. A., et al. 2006, *MNRAS*, **371**, 157
- Moffett, A. J., Kannappan, S. J., Baker, A. J., & Laine, S. 2012, *ApJ*, **745**, 34
- Moffett, A. J., Kannappan, S. J., Berlind, A. A., et al. 2015, *ApJ*, **812**, 89
- Nair, P. B., & Abraham, R. G. 2010, *ApJS*, **186**, 427
- Oosterloo, T., Morganti, R., Crocker, A., et al. 2010, *MNRAS*, **409**, 500
- Peng, C. Y., Ho, L. C., Impey, C. D., & Rix, H.-W. 2002, *AJ*, **124**, 266
- Peirani, S., Crockett, R. M., Geen, S., et al. 2010, *MNRAS*, **405**, 2327
- Quinn, P. J. 1984, *ApJ*, **279**, 596
- Reda, F. M., Forbes, D. A., Beasley, M. A., O'Sullivan, E. J., & Goudfrooij, P. 2004, *MNRAS*, **354**, 851
- Rutkowski, M. J., Jeong, H., Cohen, S. H., et al. 2014, *ApJ*, **796**, 101
- Schawinski, K., Lintott, C., Thomas, D., et al. 2009, *MNRAS*, **396**, 818
- Serra, P., & Oosterloo, T. A. 2010, *MNRAS*, **401**, L29
- Serra, P., Oser, L., Krajnović, D., et al. 2014, *MNRAS*, **444**, 3388
- Sérsic, J. L. 1968, Cordoba, Argentina: Observatorio Astronomico
- Stark, D. V., Kannappan, S. J., Wei, L. H., et al. 2013, *ApJ*, **769**, 82
- Thilker, D. A., Bianchi, L., Schiminovich, D., et al. 2010, *ApJ*, **714**, L171
- Toomre, A. 1977, Evolution of Galaxies and Stellar Populations, 401
- Trager, S. C., Faber, S. M., Worthey, G., & González, J. J. 2000, *AJ*, **120**, 165
- Trujillo, I., Ferreras, I., & de La Rosa, I. G. 2011, *MNRAS*, **415**, 3903
- van Driel, W., Arnaboldi, M., Combes, F., & Sparke, L. S. 2000, *A&AS*, **141**, 385
- van Driel, W., Combes, F., Arnaboldi, M., & Sparke, L. S. 2002, *A&A*, **386**, 140
- Vikram, V., Wadadekar, Y., Kembhavi, A. K., & Vijayagovindan, G. V. 2010, *MNRAS*, **409**, 1379
- Visvanathan, N., & Sandage, A. 1977, *ApJ*, **216**, 214
- Wei, L. H., Vogel, S. N., Kannappan, S. J., et al. 2010, *ApJ*, **725**, L62
- Willett, K. W., Lintott, C. J., Bamford, S. P., et al. 2013, *MNRAS*, **435**, 2835
- Wong, O. I., Schawinski, K., Józsa, G. I. G., et al. 2015, *MNRAS*, **447**, 3311
- Whitmore, B. C., Lucas, R. A., McElroy, D. B., et al. 1990, *AJ*, **100**, 1489
- Yi, S. K., Yoon, S.-J., Kaviraj, S., et al. 2005, *ApJ*, **619**, L111
- Young, L. M., Bureau, M., Davis, T. A., et al. 2011, *MNRAS*, **414**, 940
- Young, L. M., Scott, N., Serra, P., et al. 2014, *MNRAS*, **444**, 3408

Appendix A: Additional table

Table A.1. Details of the structural analysis of 55 Blue early-type galaxies.

S09	SDSS	RA	Dec	$z$	$M_r$	$u-r$	$SFR$	$(\mu_e)$	$(\mu_e)$	$(\mu_e)$	$ser + exp$	$Re$	$eRe$	$Re$	$ser + exp$	$Re$	$eRe$	$Re$	$ser + exp$	$n$	$en$	$n$	$ser + exp$	$en$	$b/a$	$b/a$	$ser + exp$	Residual	
ID	ID	h-m-s	d-m-s		(mag)	(mag)	( $M_{\odot}/yr$ )	(mag/arcsec <sup>2</sup> )	(mag/arcsec <sup>2</sup> )	(mag/arcsec <sup>2</sup> )	(mag/arcsec <sup>2</sup> )	(kpc)	(kpc)	(kpc)	(kpc)	(kpc)	(kpc)	(kpc)	(kpc)										feature
2	58772298272925748	11:23:27.0	-00:42:48.8	0.04084	-20.81	1.606	4.5	19.46	0.04	0.15	17.26	2.26	0.02	0.38	0.01	3.15	0.03	0.73	0.15	0.97	0.75	0.75	0.75	0.01	0.85	0.85	0.85	0.85	Stellar debris
4	58772298272925748	15:23:47.1	-00:38:23.0	0.03747	-21.0	1.908	2.5	19.48	0.05	0.22	17.79	2.32	0.03	0.65	0.01	4.22	0.04	1.03	0.01	0.85	0.83	0.83	0.83	0.01	0.85	0.85	0.85	0.85	Stellar debris
5	58772298272925748	12:08:23.5	-00:06:37.0	0.04081	-21.5	2.038	3.5	19.57	0.04	0.18	18.11	3.37	0.03	1.1	0.01	3.67	0.02	1.56	0.02	0.91	0.93	0.93	0.93	0.02	0.91	0.91	0.91	0.91	Stellar debris
7	587724198282133547	01:41:43.2	+13:40:32.8	0.04559	-21.81	1.432	12.0	18.58	0.01	0.18	18.6	2.15	0.01	1.64	0.0	0.97	0.01	0.4	0.0	0.86	0.81	0.81	0.81	0.0	0.86	0.86	0.86	0.86	Stellar debris
8	587725190351818182	10:35:58.7	+15:14:50.1	0.04176	-21.4	2.261	7.0	20.58	0.08	0.24	20.14	3.1	0.08	3.37	0.16	4.87	0.04	5.36	0.12	0.71	0.7	0.7	0.7	0.12	0.71	0.71	0.71	0.71	Stellar debris
14	58772550139408624	12:35:02.6	+66:22:33.4	0.04684	-21.67	1.959	6.1	19.23	0.11	0.16	20.42	3.62	0.08	0.71	0.01	8.0	0.11	2.3	0.04	0.81	0.75	0.75	0.75	0.11	0.75	0.75	0.75	0.75	Stellar debris
20	587725981226107027	08:29:09.1	+52:49:06.9	0.04842	-21.18	1.835	2.1	19.9	0.09	0.19	19.95	3.06	0.05	3.13	0.0	3.55	0.05	3.64	0.0	0.95	0.95	0.95	0.95	0.0	0.95	0.95	0.95	0.95	Stellar debris
23	587726031175548968	12:06:47.2	+01:17:09.8	0.04124	-21.18	2.207	1.2	19.61	0.06	0.29	20.36	3.2	0.02	0.29	0.0	1.09	0.01	6.53	0.28	0.74	0.73	0.73	0.73	0.0	0.71	0.71	0.71	0.71	Stellar debris
30	587726100953432183	15:17:19.7	+03:19:18.9	0.03749	-20.74	2.131	0.73	20.41	0.02	0.21	20.65	2.38	0.01	1.46	0.06	4.68	0.04	2.75	0.09	0.7	0.64	0.64	0.64	0.0	0.71	0.71	0.71	0.71	Stellar debris
41	587728769266502060	10:16:28.4	+03:35:02.7	0.04848	-21.72	2.38	6.1	20.65	0.07	0.18	18.63	6.48	0.09	1.46	0.0	1.09	0.01	6.53	0.28	0.74	0.73	0.73	0.73	0.0	0.71	0.71	0.71	0.71	Stellar debris
50	587731512617402577	03:50:17.5	+03:50:17.5	0.03967	-21.86	2.158	6.6	20.59	0.08	0.18	18.39	7.27	0.11	1.8	0.05	7.27	0.05	3.93	0.07	0.95	0.94	0.94	0.94	0.07	0.95	0.95	0.95	0.95	Stellar debris
52	587732411518808182	14:52:47.8	+62:00:14.6	0.04306	-21.45	2.173	3.9	19.0	0.02	0.23	19.38	2.39	0.01	15.83	4.37	1.6	0.01	8.0	0.84	0.76	0.86	0.86	0.86	0.01	0.84	0.84	0.84	0.84	Stellar debris
56	587729408622723373	17:23:24.9	+67:48:46.3	0.04845	-21.46	2.037	3.2	19.13	0.03	0.32	20.65	2.53	0.02	4.9	0.31	2.69	0.02	5.36	0.23	0.89	0.86	0.86	0.86	0.02	0.89	0.89	0.89	0.89	Stellar debris
58	58772978516820024	14:06:56.4	-01:35:41.0	0.02916	-21.37	2.127	5.7	19.08	0.01	0.20	20.55	2.28	0.01	3.54	0.07	1.59	0.0	2.63	0.05	0.51	0.61	0.61	0.61	0.0	0.51	0.51	0.51	0.51	Stellar debris
61	587730816286785893	22:15:16.2	+09:15:47.6	0.03843	-21.61	1.707	21.0	20.97	0.1	0.24	20.28	7.59	0.15	3.96	0.19	6.25	0.06	8.0	0.18	0.86	0.78	0.78	0.78	0.19	0.86	0.86	0.86	0.86	Stellar debris
66	587731500261834946	10:54:37.9	+55:39:46.0	0.04787	-20.89	1.976	6.5	20.16	0.05	0.19	19.63	3.27	0.03	2.01	0.07	2.31	0.02	1.66	0.04	0.69	0.66	0.66	0.66	0.07	0.69	0.69	0.69	0.69	Stellar debris
72	587731512617402577	03:50:17.5	+03:50:17.5	0.04285	-21.1	2.156	3.2	19.76	0.05	0.18	18.95	2.67	0.03	1.39	0.02	2.81	0.03	1.58	0.03	0.58	0.56	0.56	0.56	0.02	0.58	0.58	0.58	0.58	Stellar debris
68	58773152170730241	09:13:23.7	+43:58:34.2	0.04361	-20.77	1.893	1.4	20.31	0.03	0.32	21.35	3.19	0.02	2.86	0.17	1.17	0.01	2.03	0.16	0.65	0.57	0.57	0.57	0.01	0.65	0.65	0.65	0.65	Stellar debris
102	587733411518808182	14:52:47.8	+62:00:14.6	0.04381	-20.78	1.812	2.176	14.0	0.05	0.14	20.68	0.2	5.18	0.07	5.51	0.21	4.56	0.04	5.71	0.14	0.72	0.68	0.68	0.04	0.72	0.72	0.72	0.72	Stellar debris
103	58773341206478620	14:07:44.2	+52:38:09.7	0.04381	-20.84	2.238	0.53	19.55	0.04	0.24	20.11	2.37	0.02	2.7	0.11	2.34	0.02	3.5	0.19	0.98	0.96	0.96	0.96	0.02	0.98	0.98	0.98	0.98	Stellar debris
77	58773341206478620	12:20:37.4	+56:28:46.2	0.04381	-20.84	2.238	0.53	19.55	0.04	0.24	20.11	2.37	0.02	2.7	0.11	2.34	0.02	3.5	0.19	0.98	0.96	0.96	0.96	0.02	0.98	0.98	0.98	0.98	Stellar debris
84	587732157380013064	07:54:20.6	+25:51:33.2	0.04167	-21.06	2.021	1.7	20.43	0.14	0.14	17.08	4.56	0.13	0.54	0.01	8.0	0.12	2.71	0.11	0.86	0.81	0.81	0.81	0.12	0.86	0.86	0.86	0.86	Stellar debris
86	587732471463411876	08:53:11.4	+37:08:06.5	0.0498	-21.59	2.063	10.0	19.39	0.03	0.06	18.31	3.03	0.02	1.05	0.01	2.58	0.01	1.11	0.02	0.95	0.9	0.9	0.9	0.01	0.95	0.95	0.95	0.95	Stellar debris
91	58773276998290690	12:20:23.1	+08:51:37.1	0.04894	-20.88	2.086	3.6	19.63	0.04	0.19	19.63	2.45	0.02	1.65	0.02	2.05	0.02	1.34	0.02	0.67	0.62	0.62	0.62	0.02	0.67	0.67	0.67	0.67	Stellar debris
92	58773276998290690	12:20:23.1	+08:51:37.1	0.04894	-20.88	2.086	3.6	19.63	0.04	0.19	19.63	2.45	0.02	1.65	0.02	2.05	0.02	1.34	0.02	0.67	0.62	0.62	0.62	0.02	0.67	0.67	0.67	0.67	Stellar debris
101	587733411518808182	14:52:47.8	+62:00:14.6	0.04361	-20.77	1.893	1.4	20.31	0.03	0.32	21.35	3.19	0.02	2.86	0.17	1.17	0.01	2.03	0.16	0.65	0.57	0.57	0.57	0.01	0.65	0.65	0.65	0.65	Stellar debris
124	58773647586554950	13:47:47.7	+11:16:27.0	0.03942	-20.71	1.873	5.5	19.78	0.05	0.19	19.58	2.07	0.03	2.68	0.04	3.72	0.03	3.75	0.04	0.6	0.55	0.55	0.55	0.03	0.55	0.55	0.55	0.55	Stellar debris
121	58773647586554950	13:47:47.7	+11:16:27.0	0.03942	-20.71	1.873	5.5	19.78	0.05	0.19	19.58	2.07	0.03	2.68	0.04	3.72	0.03	3.75	0.04	0.6	0.55	0.55	0.55	0.03	0.55	0.55	0.55	0.55	Stellar debris
124	58773647586554950	13:47:47.7	+11:16:27.0	0.03942	-20.71	1.873	5.5	19.78	0.05	0.19	19.58	2.07	0.03	2.68	0.04	3.72	0.03	3.75	0.04	0.6	0.55	0.55	0.55	0.03	0.55	0.55	0.55	0.55	Stellar debris
121	58773647586554950	13:47:47.7	+11:16:27.0	0.03942	-20.71	1.873	5.5	19.78	0.05	0.19	19.58	2.07	0.03	2.68	0.04	3.72	0.03	3.75	0.04	0.6	0.55	0.55	0.55	0.03	0.55	0.55	0.55	0.55	Stellar debris
124	58773647586554950	13:47:47.7	+11:16:27.0	0.03942	-20.71	1.873	5.5	19.78	0.05	0.19	19.58	2.07	0.03	2.68	0.04	3.72	0.03	3.75	0.04	0.6	0.55	0.55	0.55	0.03	0.55	0.55	0.55	0.55	Stellar debris
121	58773647586554950	13:47:47.7	+11:16:27.0	0.03942	-20.71	1.873	5.5	19.78	0.05	0.19	19.58	2.07	0.03	2.68	0.04	3.72	0.03	3.75	0.04	0.6	0.55	0.55	0.55	0.03	0.55	0.55	0.55	0.55	Stellar debris
124	58773647586554950	13:47:47.7	+11:16:27.0	0.03942	-20.71	1.873	5.5	19.78	0.05	0.19	19.58	2.07	0.03	2.68	0.04	3.72	0.03	3.75	0.04	0.6	0.55	0.55	0.55	0.03	0.55	0.55	0.55	0.55	Stellar debris
121	58773647586554950	13:47:47.7	+11:16:27.0	0.03942	-20.71	1.873	5.5	19.78	0.05	0.19	19.58	2.07	0.03	2.68	0.04	3.72	0.03	3.75	0.04	0.6	0.55	0.55	0.55	0.03	0.55	0.55	0.55	0.55	Stellar debris
124	58773647586554950	13:47:47.7	+11:16:27.0	0.03942	-20.71	1.873	5.5	19.78	0.05	0.19	19.58	2.07	0.03	2.68	0.04	3.72	0.03	3.75	0.04	0.6									